4A.1

The Vertical Vorticity Structure within a Squall Line Observed during BAMEX: Banded Vorticity Features and the Evolution of a Bowing Segment

Roger M. Wakimoto

National Science Foundation
Arlington, CA 22230

1. Introduction

The vertical vorticity structure has been shown to significantly influence the evolution of mesoscale convective systems (e.g., Verlinde and Cotton 1990, Bartels and Maddox 1991, Biggerstaff and Houze 1991b, Weisman 1993, Davis and Weisman 1994, Skamarock et al. 1994, Weisman and Davis 1998). Previous studies have shown a wide variety of vortices that vary in horizontal dimensions and exist for hours to several days. The latter circulation type can exist beyond the life cycle of the parent convective system. Of particular interest in this study are the smaller-scale vortices that occur within quasi-linear convective systems, i.e., a mesoscale system associated with a convective line that is approximate linear. Vortices in these systems can locally enhance the strength of rear inflow jets (e.g., Smull and Houze 1987, Weisman 1992) and contribute to the development of long-lived, balanced mesoscale convective vortices (MCVs; Davis and Trier 2002).

The large-scale balanced midlevel circulation (100-600 km in diameter) is typically found in the stratiform region of convective systems (e.g., Houze et al. 1989, Houze et al. 1990) and can initiate new convection on subsequent days (e.g., Bartels and Maddox 1991, Bosart and Sanders 1981, Fritsch et al. 1994). This vortex is such a common feature within these systems that other vorticity structures have rarely been reported in the literature. Biggerstaff and Houze (1991a and b) were the first to document prominent bands or ribbons of positive and negative vertical vorticity oriented parallel to the convective line and extending into the stratiform region. Their results were based on a composite analysis of dual-Doppler data, rawindsonde winds, wind profilers and surface mesonet observations that were digitized onto a 15 x 15 km^2 grid and filtered to remove wavelengths less than 60 km. A model simulation of the same storm by Zhang et al. (1989) replicated the banded structure. Biggerstaff and Houze (1991b) hypothesized that coarse horizontal resolution may have prevented past studies from documenting this kinematic structure. However, to the authors' knowledge, there has been no subsequent observational study that has documented a similar event even with the availability of higher spatial resolution data collected by both mobile ground-based and airborne Doppler radars.

Mesoscale vortices that are counter-rotating are characteristic features of bow echoes (e.g., Fujita 1981, Weisman 2001) and are also referred to as bookend or line end vortices (Weisman 1993). Bow echoes are observed over a range of scales from tens to a few hundred kilometers (Klimowski et al. 2004). Bow echoes can occur as isolated features or as smaller-scale bow-shaped segments within a larger squall line (e.g., Johns and Hirt 1987, Przybylinski 1995). Weisman and Davis (1998) referred to the latter circulations as subsystem-scale vortices. These segments are 15-40 km in length and were more recently modeled by James et al. (2006). Although these bow-shaped segments have been recognized to exist for a number of years, there has been no detailed observational study that has examined this type of event. On 2 June 2003, a quasi-linear convective line with a trailing stratiform region developed over Mississippi while being sampled by two airborne Doppler radars during the Bow Echo and MCV Experiment (BAMEX; Davis et al. 2004). The radars onboard the aircraft collected finescale reflectivity and Doppler velocities that documented the evolution of the convective line while also capturing the development of a ~40 km bowing segment with the line.

2. BAMEX

One of the major objectives of the BAMEX field campaign was to collect data on the life cycle of bow echo systems that are associated with damaging winds at the surface. The field phase of the experiment was the spring and summer of 2003 and was based at MidAmerica Airport located east of St. Louis, Missouri. The primary platforms used in the current study are two airborne Doppler radars that have been used extensively to study convective phenomenon.

3. Environmental conditions, overview of the quasi-linear convective system, and the aircraft flight legs

The low-level wind shear was examined based on a sounding (not shown), a nearby wind profiler, and a number of velocity azimuth display (VAD) analyses from the Doppler velocity data collected by the WSR-88D located at KGWX. The profiler and VAD analysis provided a consistent estimate of the low-level wind shear (Fig. 1). The black and dashed lines on the figure approximate the 0-3.5 km wind shear and suggests that it was ~21 m s^{-1} (Fig. 1). This value is within the range that could support bow echoes (e.g., Evans and Doswell 2001, Coniglio et al. 2004). The wind profile based on the sounding was

* Corresponding author address: Roger M. Wakimoto, NSF, 4201 Wilson Blvd., Room 705, Arlington, VA 22230; e-mail: rwakimot@nsf.gov

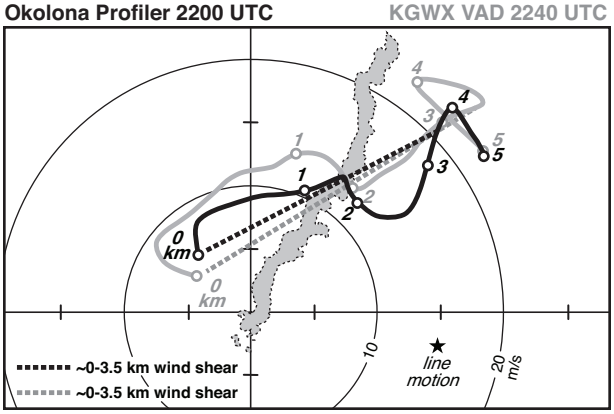

Fig. 1. Hodographs showing the 0-3.5 km AGL shear based on data from the Okolona profiler at 2200 UTC (black line) and a VAD analysis of the KGWX WSR-88D radar data at 2240 UTC (gray line). The black dashed and gray dashed lines represent the approximate 0-3.5 km shear based on the profiler and radar data, respectively. Radar reflectivities greater than 35 dBZ at 2306:00-2325:00 UTC are shaded gray. The star represents the convective line motion. Location of the Okolona profiler is shown in Fig. 2.

not used since it did not depict the southeasterly flow at the surface that was apparent in the other wind profiles and the surface analyses of the winds in eastern Arkansas and northern Mississippi (not shown).

The outline of the convective line at 2306:00-2325:00 UTC (hereafter; all times are UTC) is also plotted in Fig. 1 and reveals that a substantial component of the low-level shear vector was parallel to the quasi-linear convective line (hereafter; referred to as the convective line). The relationship between squall line orientation and low-level shear vector has received a great deal of attention in the literature. The tendency for the low-level shear vector to align perpendicular to the convective lines has been noted (e.g., Bluestein and Jain 1985, Rotunno et al. 1988, Weisman et al. 1988, Keenan and Carbone 1992, Fankhauser et al. 1992, Weisman 1993, Robe and Emanuel 2001). However, convective lines can also be associated with a significant component of the low-level wind shear along the line (e.g., Parker and Johnson 2000).

A sequence of low-level scans from the nearby KGWX radar is presented in Fig. 2. The line movement shown in the figure was ~15 m s^{-1} from 260°. The arrow (Fig. 2g) denotes the location where a small-scale bow echo develops. Strong winds (sustained speeds greater than 30 m s^{-1}) and minor damage were reported as the bowing segment moved into eastern Mississippi. Also plotted on the figure are the flight tracks of ELDORA and the NOAA P-3. The convective line was sampled by the airborne platforms for over 2 hours providing good time history of the mesoscale system and also documenting the formation of the bow echo.

4. Multiple Doppler analyses

a. Overall structure of the convective line

1) 2214:18 – 2229:00 UTC

The first analysis of the convective line is from 2214 – 2229 (Fig. 3a) and combines the wind syntheses of both ELDORA and the NOAA P-3 radars. An examination of the wind syntheses revealed that the vertical vorticity features were well-defined at the 2.25 km level. There is general southeasterly storm-relative flow ahead of the convective line. The flow to the rear of the convective line reveals weak southwesterly flow followed by a region of stronger northeasterly winds before the winds turn to become southerly to southwesterly much farther to the west. This alternating pattern in the wind field is consistent with the distinct bands of vertical vorticity (Fig. 3b) starting with a ribbon of cyclonic vorticity within the convective line followed by anticyclonic, cyclonic and anticyclonic bands further into the stratiform region. There is also a weak band of anticyclonic vorticity out ahead of the convective line also shown in Biggerstaff and Houze (1991b) although it is not discussed (see their Fig. 3).

Biggerstaff and Houze (1991a and b) are the only known observational studies that have shown this type of alternating ribbons of vertical vorticity within a squall line. They used a composite analysis of several data sources over an approximate 3-hour period. The present case was able to examine the structure of these vorticity features with higher temporal resolution. The widths of the individual bands documented in their study were ~60 km, much greater than the organization shown in Fig. 3b. Zhang et al. (1989) performed a numerical simulation of the same squall line and appeared to replicate the banded structure. Trier et al. (1997) simulated a tropical squall line that also exhibited a band of cyclonic vorticity followed by an anticyclonic band (see their Fig. 16) although it is not discussed since their focus was on the formation of line-end vortices.

The vertical velocity field (Fig. 3c) for this time also shows a banded structure which suggests that tilting of horizontal vorticity could be playing a role in creating the observed vertical vorticity field. The horizontal vorticity vectors out ahead of the convective line (Fig. 3c) are pointing to the northwest consistent with the low-level shear depicted in the hodograph (Fig. 1). Accordingly, there is a significant component of the horizontal vorticity vector that is perpendicular to the line. The tilting of vorticity is shown in Fig. 3d also suggests a structure consistent with the vertical vorticity plot.

The vertical cross section oriented in a direction perpendicular to the convective line is presented in Fig. 4. The results shown in this figure depict the mean vertical structure by averaging individual vertical cross section from the Doppler wind syntheses along the entire length of the flight track.

The storm-relative flow and radar reflectivity profiles (Fig. 4a and b) are largely consistent with midlatitude mesoscale convective systems documented in the literature (e.g., Houze et al. 1989). A leading convective line followed by a transition zone and stratiform region with a bright band are apparent. An ascending front-to-rear flow is evident in the cross section although no rear inflow can

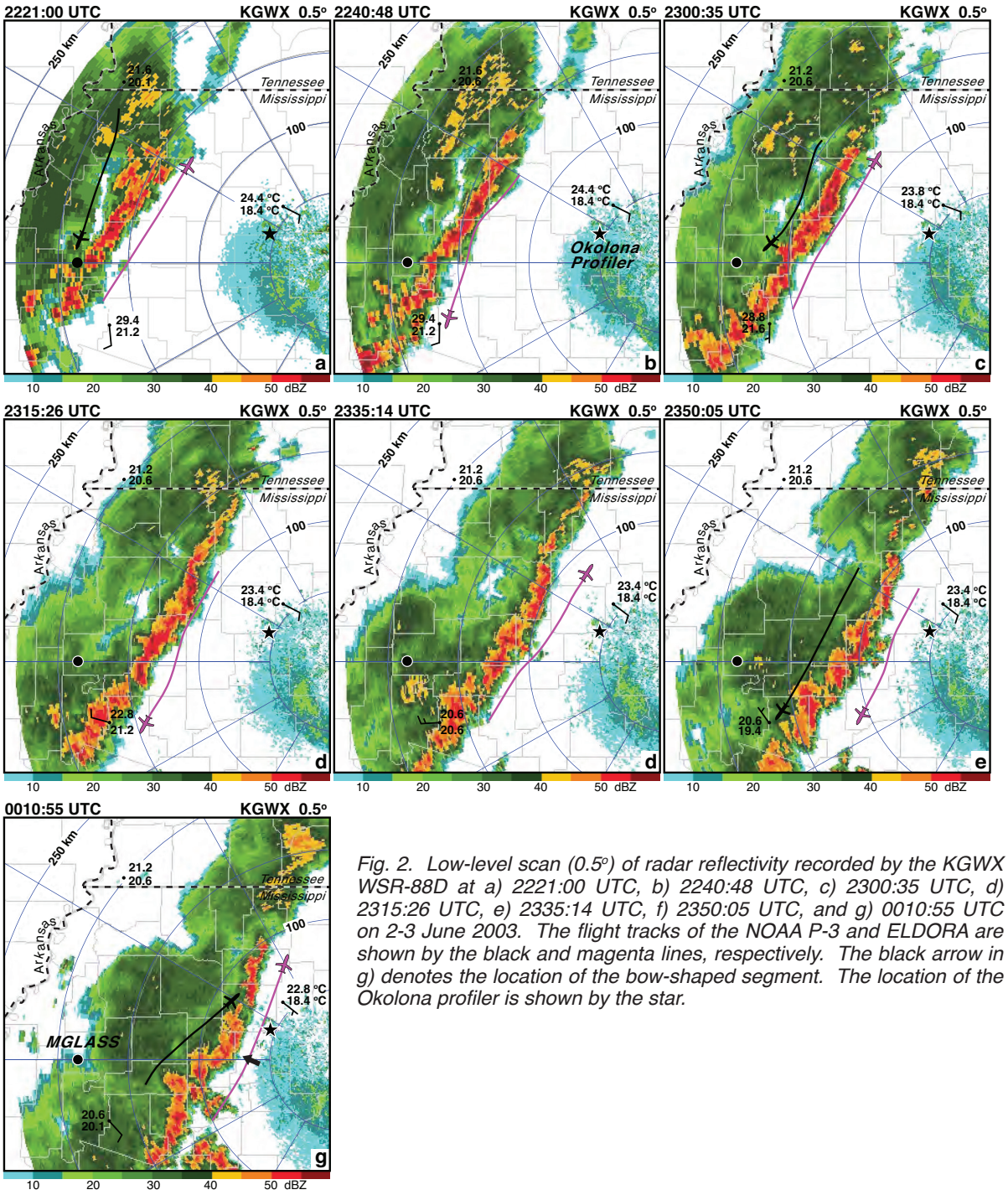

Fig. 2. Low-level scan (0.5°) of radar reflectivity recorded by the KGWX WSR-88D at a) 2221:00 UTC, b) 2240:48 UTC, c) 2300:35 UTC, d) 2315:26 UTC, e) 2335:14 UTC, f) 2350:05 UTC, and g) 0010:55 UTC on 2-3 June 2003. The flight tracks of the NOAA P-3 and ELDORA are shown by the black and magenta lines, respectively. The black arrow in g) denotes the location of the bow-shaped segment. The location of the Okolona profiler is shown by the star.

be identified at this time. The vertical velocity field and vorticity vectors shown in Fig. 4c strongly suggest tilting as the primary mechanism for the banded vertical vorticity structure shown in Fig. 3b. This is further supported by the comparison of the tilting and vertical vorticity plots (Fig. 4d). There appears to be three general areas of downward motion depicted in the mean cross sections (Fig. 4c). The first is the low-level downdraft embedded within the leading convective line. Downdrafts are also noted within the transition zone and near the bright band associated with the region of stratiform precipitation. The latter two downdrafts have been well documented (e.g., Biggerstaff and Houze 1991b). In addition, another downdraft is apparent ahead of the convective region and is believed to be associated with subsidence (Hoxit et al. 1976, Sun et al. 1976). This downdraft contributes to the development of the anticyclonic band of ahead of the convective line by the downward tilting of the ambient horizontal vorticity.

The results presented in Figs. 3 and 4 are con-

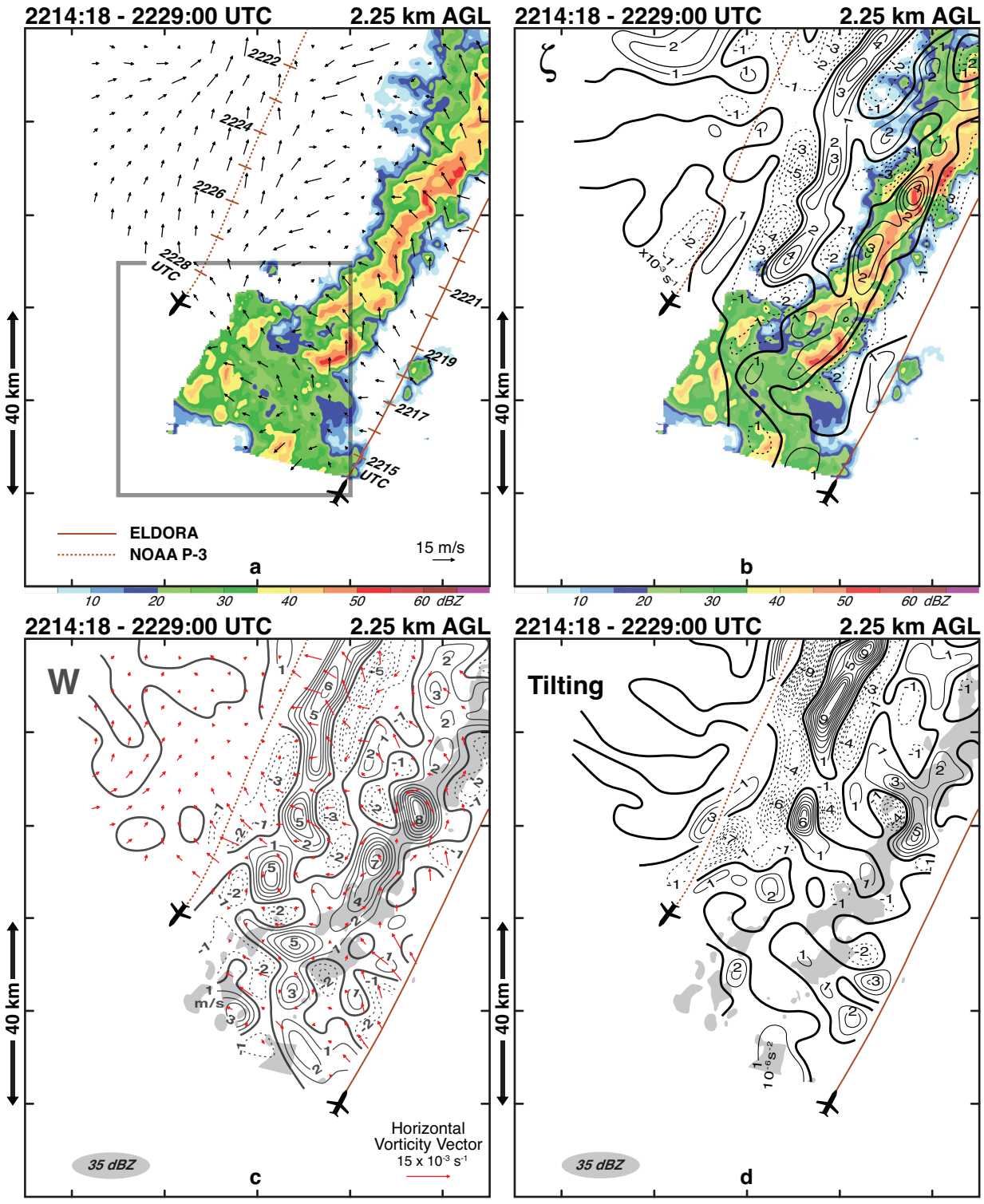

Fig. 3. Wind synthesis at 2214:18 – 2229:00 UTC at 2.25 km AGL. (a) Storm-relative winds and radar reflectivity. (b) Vertical vorticity (x10^{-3} s^{-1}) and radar reflectivity. (c) Horizontal vorticity vectors, vertical velocity, and radar reflectivities >35 dBZ shaded gray (d) tilting term (x10^{-6} s^{-2}) and radar reflectivities >35 dBZ shaded gray. ELDORA and the NOAA P-3 flight tracks are shown by the solid and dashed brown lines, respectively. Positive and negative values of vertical vorticity, vertical velocity, and tilting term are shown by the solid and dashed black lines, respectively. The box represents the region where the bow echo will develop.

sistent with the vorticity structure at lower levels presented by Biggerstaff and Houze (1991b) with two differences. The tilting of the horizontal vorticity by the low-level convective downdraft and the downdraft associated with

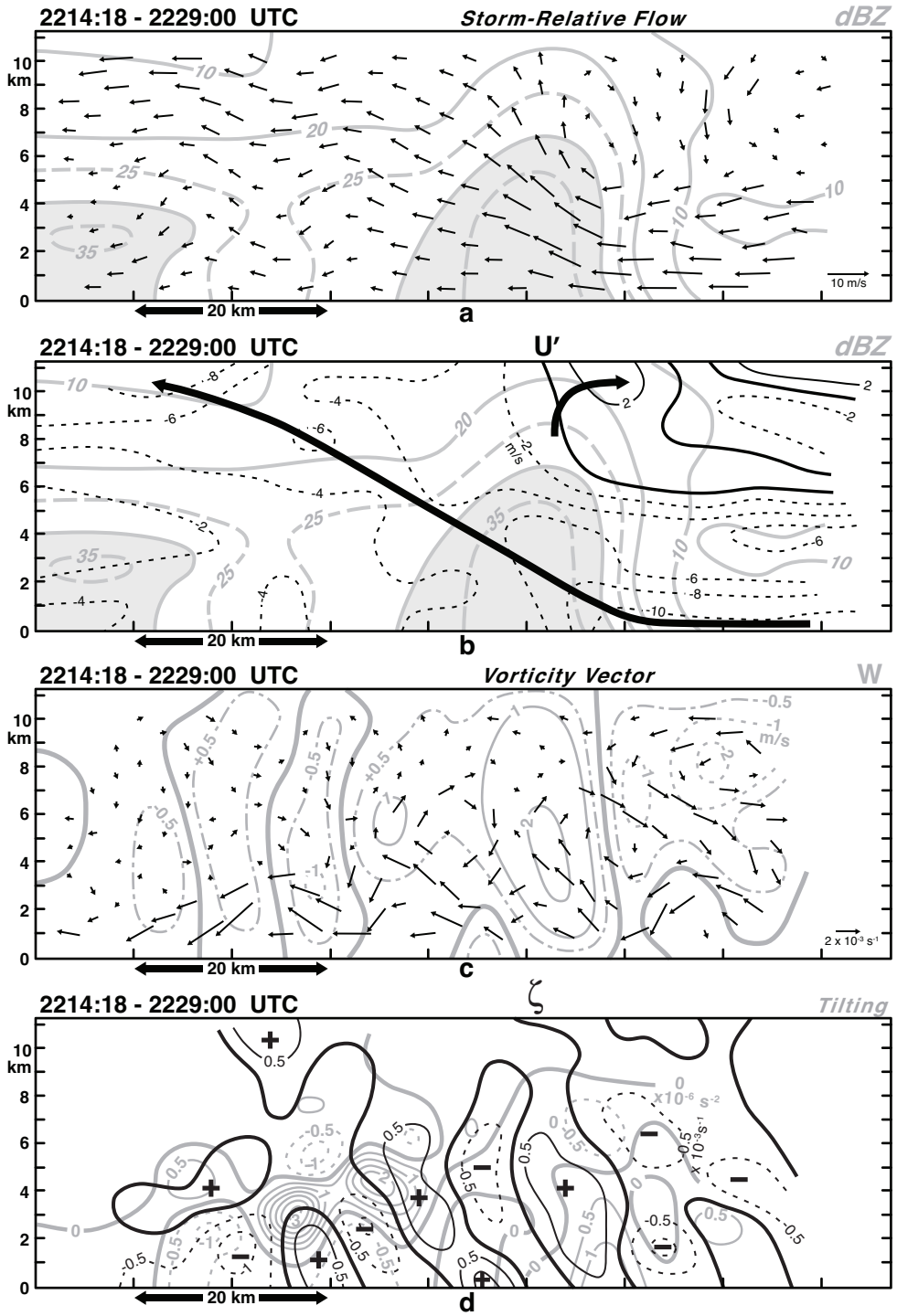

Fig. 4. Vertical cross section perpendicular to the convective line at 2214:18 – 2229:00 UTC depicting (a) storm-relative flow and radar reflectivity, (b) the component of storm-relative flow perpendicular to the convective line (U') and radar reflectivity, (c) vorticity vector in the plane of the cross section and vertical velocity, and (d) vertical vorticity and tilting term. Black arrows in (b) depict approximate flow pattern as shown in (a).

the subsidence downdraft. It is likely that both of the features were present in their study but were not resolved by the coarser resolution data set.

2) 0002:45 – 0017:30 UTC

The two airborne Doppler radars were able to coordinate during the seventh pass by the convective line at 0002 – 0017. The bow echo has continued to evolve

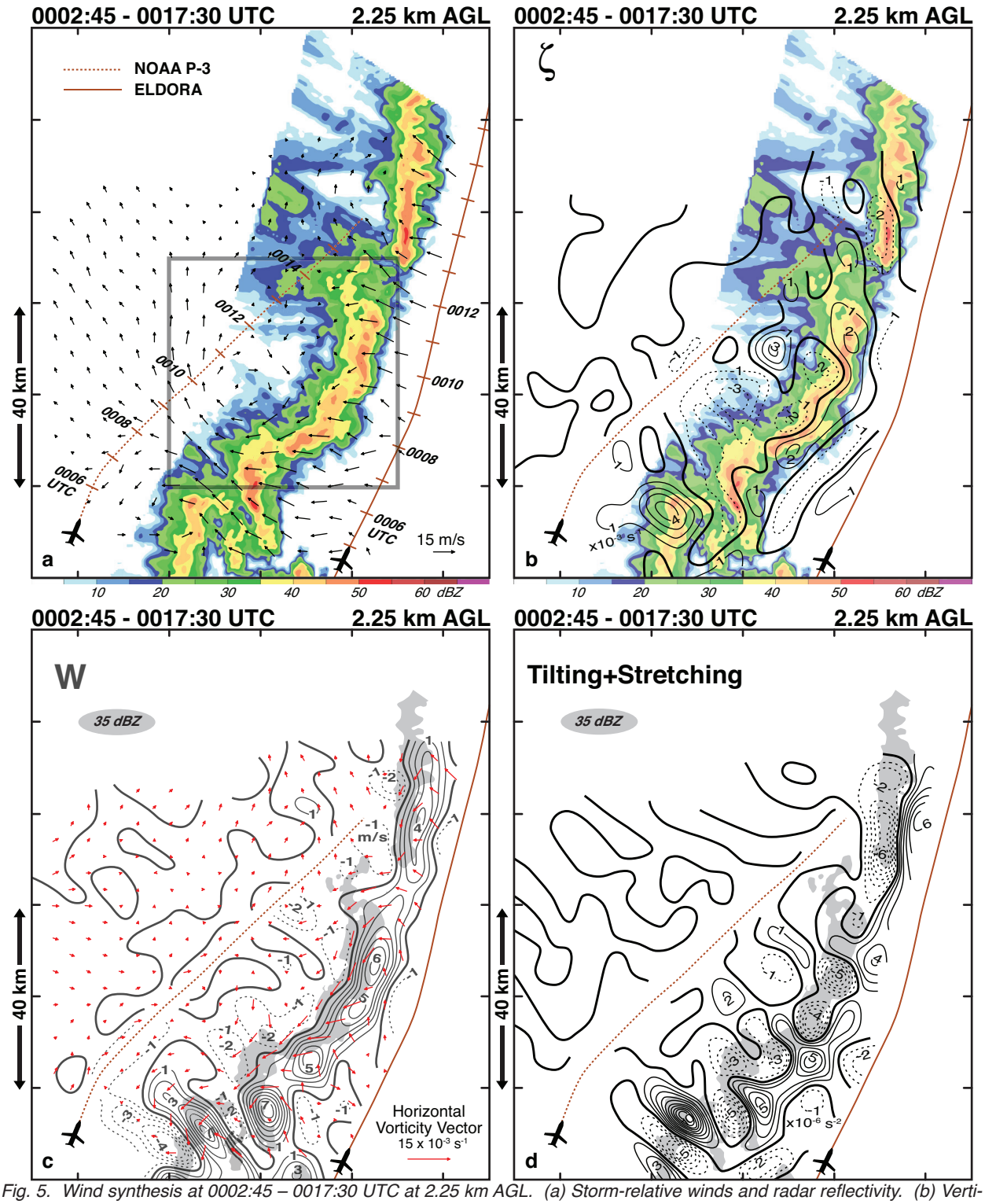

Fig. 5. Wind synthesis at 0002:45 – 0017:30 UTC at 2.25 km AGL. (a) Storm-relative winds and radar reflectivity. (b) Vertical vorticity (x10^{-3} s^{-1}) and radar reflectivity. (c) Horizontal vorticity vectors, vertical velocity, and radar reflectivities >35 dBZ shaded gray (d) tilting plus stretching terms (x10^{-6} s^{-2}) and radar reflectivities >35 dBZ shaded gray. The ELDORA and NOAA P-3 flight tracks are shown by the solid and dashed brown lines, respectively. Positive and negative values of vertical vorticity, vertical velocity, and tilting plus stretching terms are shown by the solid and dashed black lines, respectively.

and is enclosed by the box in Fig. 5a. The rear inflow into the bow apex can be seen and is flanked by the two counter-rotating vorticity circulations (Fig. 5b). An updraft followed by a region of downdraft is apparent (Fig. 5c). Further to the rear, however, the banded structure of vertical motion no longer exists. This has also resulted in a

much weaker tilting and stretching field in the stratiform region (Fig. 5d) and a more uniform distribution of vertical vorticity that no longer suggests a banded structure.

2) Discussion

The low-level wind shear vector within the environment was associated with a significant along-line component in the present study. This resulted in a horizontal vorticity vector that pointed into the convective line. The vertical motions within the convective and stratiform regions were typical for mesoscale convective systems. Downdrafts were located out ahead of the line, accompanying the heavy precipitation within the convective line, in the transition zone, and near the bright band region where the heaviest stratiform precipitation occurs. These downdrafts and the main convective updraft tilted the horizontal vorticity vector into the vertical producing prominent bands of cyclonic and anticyclonic vertical vorticity. Stretching also contributed to the maintenance of these bands. This type of vertical vorticity structure has rarely been seen in the literature. Biggerstaff and Houze (1991 a and b) also noted a similar pattern using a composite analysis. Their technique was not able to resolve the subsidence downdraft out ahead of the convective line and the low-level convective downdraft although it is likely that both were present in their case study. They were also only able to analyze one time versus the numerous Doppler radar wind syntheses available in the present study. A schematic model summarizing the vorticity patterns within this system is presented in Fig. 6.

b. The bow echo

The analyses of a convective line presented in section 4a depicts a pronounced banded structure of vertical vorticity oriented parallel to the line. This approximate two-dimensional structure changes with time as at least one segment of the line evolves into a bow echo. Embedded bow echoes (or bow-shaped segments) have been known to exist for a number of years, however, to date there has not been detailed observational examination of their life cycle. The gray box shown in Figs. 3a, and 5a denote the region where the bow echo develops along the convective line. As shown in Fig. 3, the airborne Doppler radars were able to collect data in an area primarily associated with stratiform precipitation before the a convective line formed. Accordingly, the entire evolution of the bow echo was documented.

1) 2231:00 – 2248:00 UTC

The second pass by the convective line was at 2231 - 2248. The area enlarged in Fig. 7 highlights the segment of the line that evolves into a bow echo. The previous pass by the aircraft did not reveal any incipient circulations that might be associated with a bow echo (not shown). However, counter-rotating circulations were clearly apparent during the time interval shown in Fig. 7b. The circulations are oriented southwest to northeast and the centers are separated by ~20 km. An updraft (>5 m s^{-1}) within the convective line has developed approximately between the two centers (Fig. 7c). The horizontal vorticity vectors within this updraft are primarily pointing to the southwest (Figs. 7b and c). Tilting (and subsequent stretching) of this vorticity vector would be consistent with the development of the cyclonic and anticyclonic circulations which is supported by the analysis of these terms in Fig. 7d (note the maximum and minimum centers within the convective line >4 x 10^{-6} s^{-2} and <-5 x 10^{-6} s^{-2}, respectively).

Weisman and Davis (1998) have suggested that subsystem vortices may form as a result of upward tilting of the cold-pool generated vorticity. James et al. (2006)

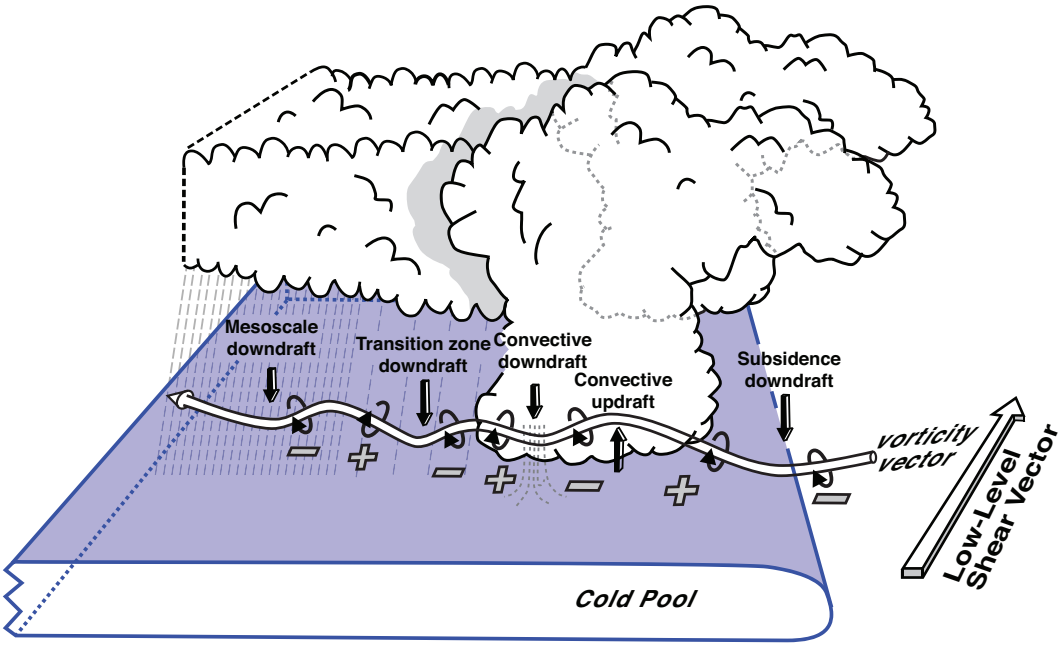

Fig. 6. Schematic model summarizing the tilting of ambient horizontal vorticity by the vertical motions within a mesoscale convective system. The plus and minus signs denote the regions of vertical vorticity that are created.

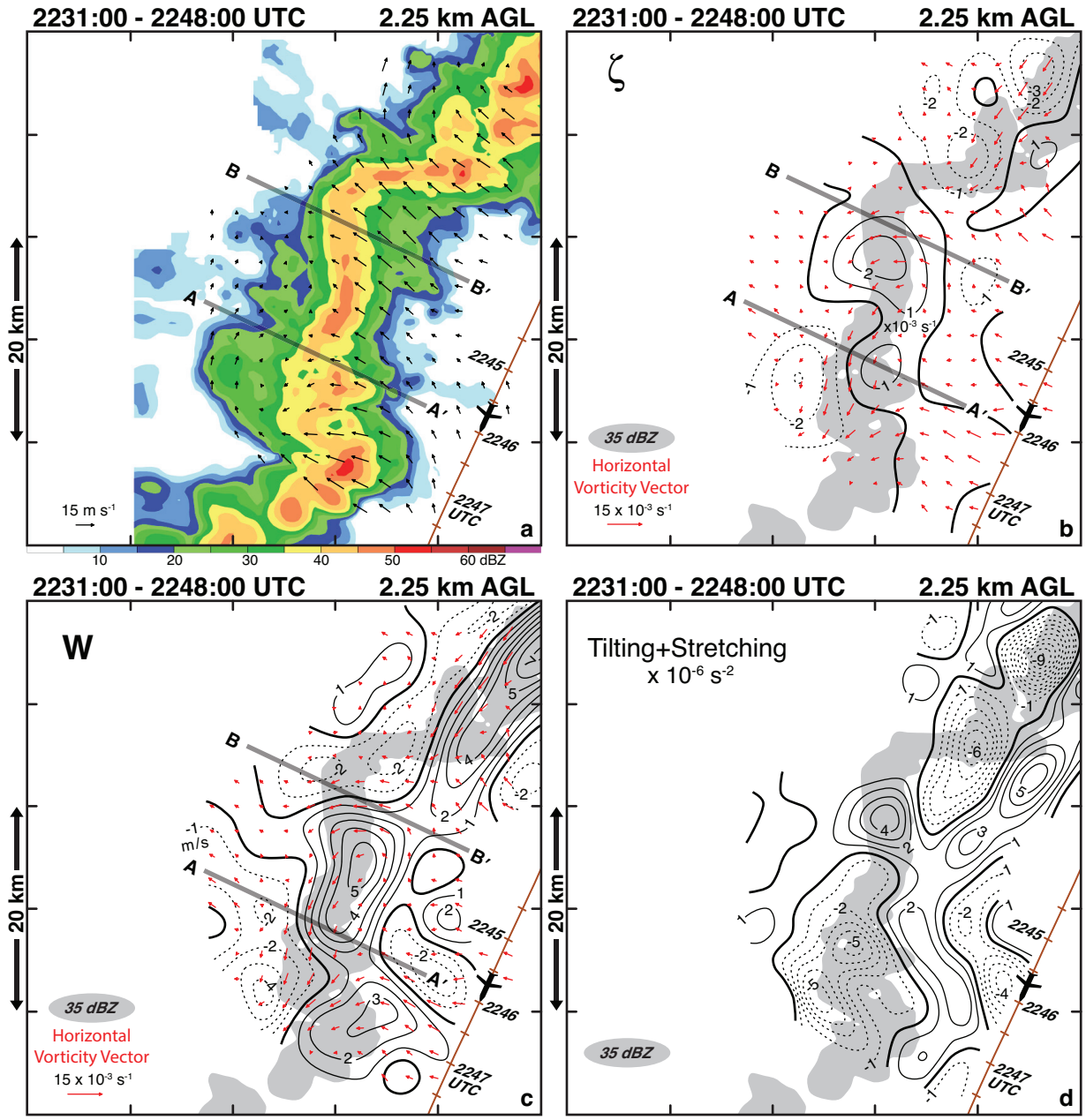

Fig. 7. Wind synthesis at 2231:00 – 2248:00 UTC at 2.25 km AGL. (a) Storm-relative winds and radar reflectivity. (b) Vertical vorticity (x 10^{-3} s^{-1}), horizontal vorticity vectors and radar reflectivities >35 dBZ shaded gray. (c) Horizontal vorticity vectors, vertical velocity, and radar reflectivities >35 dBZ shaded gray. (d) Tilting plus stretching terms (x10^{-6} s^{-2}) and radar reflectivities >35 dBZ shaded gray. ELDORA flight track is shown by the brown lines. Positive and negative values of vertical vorticity, vertical velocity, and tilting plus stretching are shown by the solid and dashed black lines, respectively. The gray lines labeled AA' and BB' denote the locations of vertical cross sections shown in Fig. 8.

have proposed that bowing segments develop at regions where the cold pool is much stronger than at other locations along the line. The analyses shown in Fig. 7 would support tilting of horizontal vorticity generated by the cold pool owing to the northeast to southwest orientation of the vorticity vector within the updraft. The vorticity vectors point in a westerly direction further north along the line before reorienting and pointing back to the southwest in the northeast section of the domain. These changes in the direction of the vector can be explained by variations in the cold pool strength along the convective line as hypothesized by James et al. (2006).

Two vertical cross sections perpendicular to the line were created to examine the cold pool structure (Fig. 8). The cross section labeled AA' is chosen to approximately where the vorticity vectors have the greatest magnitude while pointing to the southwest (Fig. 7c). The section slices through the updraft (Fig. 7c) and approximately between the two counterrotating circulations (Fig. 7b). The cross section labeled BB' is located in the area

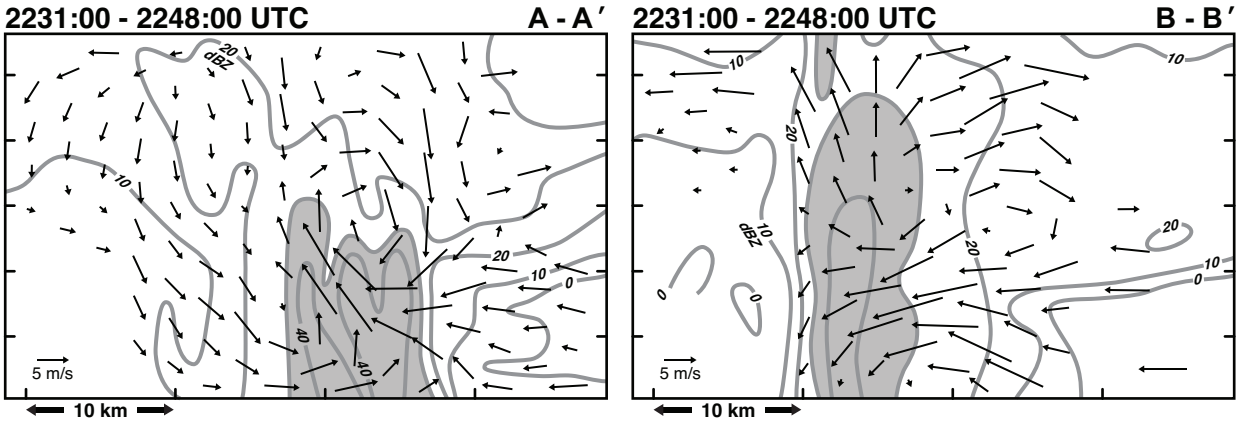

Fig. 8. Vertical cross sections perpendicular to the convective line at 2231:00 – 2248:00 UTC. The left and right panels are the sections along segment AA' and BB', respectively, shown in Fig. 7. The storm-relative winds and radar reflectivity (>35 dBZ shaded gray) are plotted.

where the vorticity vectors are pointing to the west (Fig. 7c). The storm-relative winds plotted in left panel (AA') in Fig. 8 shows the low-level outflow undercutting the inflow and leading to an upshear-tilted updraft. The negative vertical velocities at upper levels and to the rear of the convective line are associated with transition zone downdraft. The vertical cross section along BB' depicts a very shallow cold pool as expected.

2) 2344:30 – 0001:30 UTC and 0002:45 – 0017:30 UTC

The evolution of the counter-rotating circulations are shown for the last two flight legs flown by the bow echo (Fig. 9). The horizontal vorticity vector along the convective line can be used as a proxy for the strength of the cold pool. The vectors in Fig. 9a are primarily oriented northeast to southwest and are approximately the same magnitude suggesting the cold pool is uniformly strong. The tilting and stretching terms (not shown) continue to support the increase in intensity of the counter-rotating vortices noted in Fig. 7b. The vortices are persistent features for the two times shown in Fig. 9. They are close to the convective line at the earlier times (e.g., Fig. 7) and subsequently move to the rear as the echo begins to "bow out" (Fig. 9). High winds at the surface were reported during this time.

This is believed to be the first observational study that confirms the earlier numerical simulations that suggest that subsystem bow echoes are created by tilting of cold-pool generated horizontal vorticity (Weisman and Davis (1998). Preferential development occurs in regions where there is local strengthening of the cold pool (James et al. 2006). The latter study propose that bow echoes develop after the cold pool strengthens to the point where it balances the environmental shear. The convection tilts upshear and promotes local strengthening of the rear inflow. In the current study it appears that this evolution can also result in regions characterized by strong tilting and stretching of horizontal vorticity that subsequently produce counter-rotating circulations that promote rear inflow. Regions along a convective line associated with the largest values of tilting and stretching would preferentially occur where the horizontal vorticity vector and updrafts are strong (i.e., where the cold pool is deep). A schematic model summarizing the formation of the courter-rotating vortices is shown in Fig. 10.

Acknowledgments: This material is based upon work supported while serving at the National Science Foundation. Any opinion, findings, and conclusions or recommendations expressed in this material are those of the author and do not necessarily reflect the views of the National Science Foundation.

References

Bartels, D.L., and R.A. Maddox, 1991: Midlevel cyclonic vortices generated by mesoscale convective complexes. *Mon. Wea. Rev.*, **119,** 104-118.

Biggerstaff, M.I., and R.A. Houze, 1991a: Kinematic and precipitation structure of the 10-11 June 1985 squall line. *Mon. Wea. Rev.*, **119,** 3034-3065.

_____, and _____, 1991b: Midlevel vorticity structure of the 10-11 June 1985 squall line. *Mon. Wea. Rev.*, **119,** 3066-3079.

Bluestein, H.B., and M.H. Jain, 1985: Formation of mesoscale lines of precipitation: Severe squall lines in Oklahoma during the spring. *Mon. Wea. Rev.*, **42,** 1711-1732.

Bosart, L.F., and F. Sanders, 1981: The Johnstown flood of July 1977: A long-lived convective system. *J. Atmos. Sci.*, **38,** 1616-1642.

Coniglio, M.C., D.J. Stensrud, and M.B. Richman, 2004: An observational study of derecho-producing convective storms. *Wea. Forecasting*, **19,** 320-337.

Davis, C.A., and M.L. Weisman, 1994: Balanced dynamics of mesoscale vortices produced in simulated convective systems. *J. Atmos. Sci.*, **51,** 2005-2030.

_____, and S.B. Trier, 2002: Cloud-resolving simulations of mesoscale vortex intensification and its effect on a serial mesoscale convective system. *Mon. Wea. Rev.*, **130,** 2839-2858.

Davis, C., N. Atkins, D. Bartels, L. Bosart, M. Coniglio, G. Bryan, W. Cotton, D. Dowell, B. Jewett, R. Johns, D. Jorgensen, J. Knievel, K. Knupp, W.-C. Lee, G. McFarquhar, J. Moore, R. Przybylinski, R. Rauber, B. Smull, R. Trapp, S. Trier, R. Wakimoto, M. Weisman, and C. Ziegler, 2004: The bow echo and MCV experiment. *Bull. Amer. Meteor. Soc.*, **85,** 1075-1093.

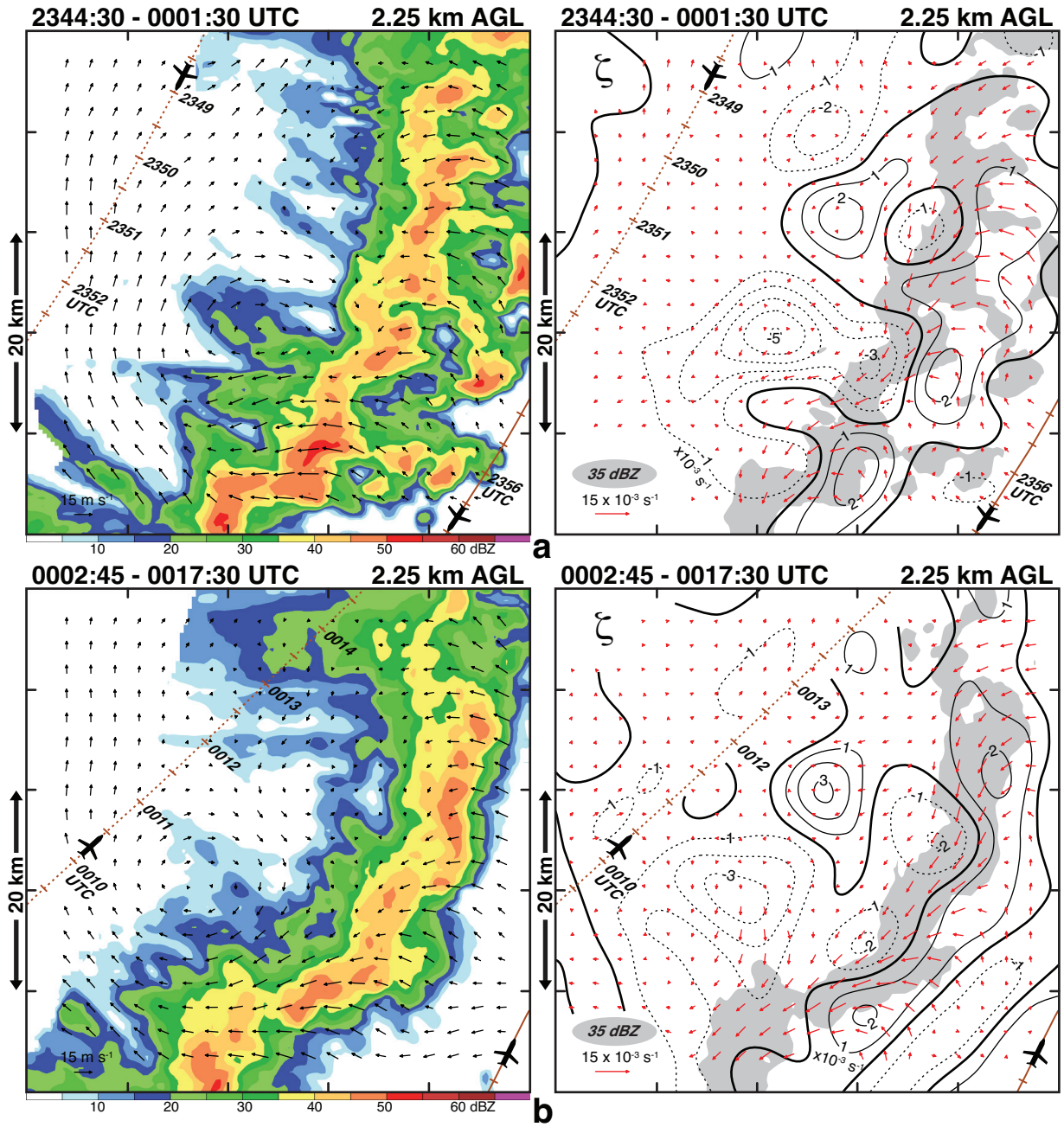

Fig. 9. Wind synthesis at (a) 2344:30 – 0001:30 UTC, and (b) 0002:45 – 0017:30 UTC at 2.25 km AGL. Left panel: Storm-relative winds and radar reflectivity. Right panel: Vertical vorticity (x 10^{-3} s^{-1}), horizontal vorticity vectors and radar reflectivities >35 dBZ shaded gray. ELDORA and NOAA P-3 flight tracks are shown by the brown and dashed brown lines, respectively. Positive and negative values of vertical vorticity, vertical velocity are shown by the solid and dashed black lines, respectively.

Evans, J.S., and C.A. Doswell III 2001: Examination of derecho environments using proximity soundings. *Wea. Forecasting*, **16,** 329-342.

Fankhauser, J.C., G.M. Barnes, and M.A. LeMone, 1992: Structure of a midlatitude squall line formed in strong unidirectional shear. *Mon. Wea. Rev.*, **120,** 237-260.

Fritsch, J.M., J.D. Murphy, and J.S. Kain, 1994: Warm core vortex amplification over land. *J. Atmos. Sci.*, **51,** 1780-1807.

Fujita, T.T., 1981: Tornadoes and downbursts in the context of generalized planetary scales. *J. Atmos. Sci.*, **38,** 1511-1534.

Houze, R.A., S.A. Rutledge, M.I. Biggerstaff, and B.F. Smull, 1989: Interpretation of Doppler weather radar displays of midlatitude mesoscale convective systems. *Bull. Amer. Meteor. Soc.*, **70,** 608-619.

_____, B.F. Smull, and P. Dodge, 1990: Mesoscale organization of springtime rainstorms in Oklahoma. *Mon. Wea. Rev.*, **118,** 613-654.

Hoxit, L.R., C.F. Chappell, and J.M. Fritsch, 1976: Formation of mesolows or pressure troughs in advance of cumulonimbus clouds. *Mon. Wea. Rev.,* **104,** 1419-1428.

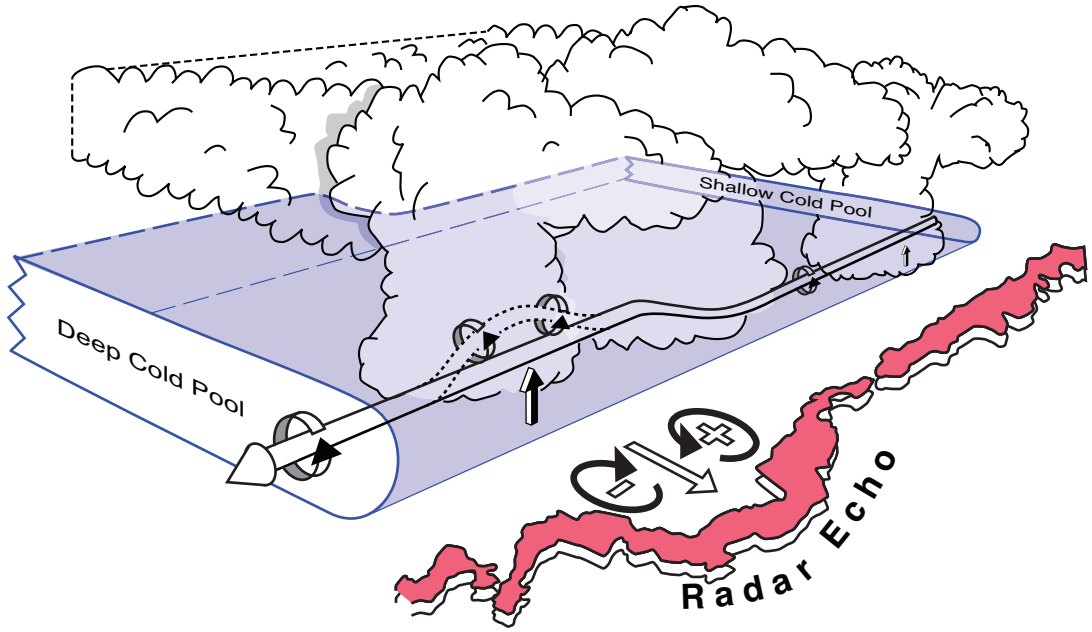

Fig. 10. Schematic model depicting the main features in the development of a bow echo embedded within a convective line. The bow echo develops in an area where the cold pool is intense (i.e., deepest). Strong horizontal vorticity and updrafts lead to the development of counter-rotating circulations produced via tilting and stretching.

James, R.P., P.M. Markowski, and J.M. Fritsch, 2006: Bow echo sensitivity to ambient moisture and cold pool strength. *Mon. Wea. Rev.*, **134,** 950-964.

_____, and W.D. Hirt, 1987: Derechos: Widespread convectively induced windstorms. *Wea. Forecasting*, **2,** 32-49.

Keenan, T.D., and R.E. Carbone, 1992: A preliminary morphology of precipitation systems in tropical northern Australia. *Quart. J. Roy. Meteor. Soc.*, **118,** 283-326.

Klimowski, B.A., M.R. Hjelmfelt, and M.J. Bunkers, 2004: Radar observations of the early evolution of bow echoes. *Wea. Forecasting*, **19,** 727-734.

Parker, M.D., and R.H. Johnson, 2000: Organizational modes of midlatitude mesoscale convective systems. *Mon. Wea. Rev.*, **128,** 3413-3436.

Przybylinski, R.W., 1995: The bow echo: Observations, numerical simulations, and severe weather detection methods. *Wea. Forecasting,* **10,** 203-218.

Robe, F., and K.A. Emanuel, 2001: The effect of vertical wind shear on radiative-convective equilibrium states. *J. Atmos. Sci.*, **58,** 1427-1445.

Rotunno, R., J.B. Klemp, and M.L. Weisman, 1988: A theory for strong, long-lived squall lines. *J. Atmos. Sci.*, **45,** 463-485.

Skamarock, W.C., M.L. Weisman, and J.B. Klemp, 1994: Three-dimensional evolution of simulated long-lived squall lines. *J. Atmos. Sci.*, **51,** 2563-2584.

Smull, B.F., and R.A. Houze, 1987: Rear inflow in squall lines with trailing stratiform precipitation. *Mon. Wea. Rev.*, **115,** 2869-2889.

Sun, J., S. Braun, M.I. Biggerstaff, R.G. Fovell, and R.A. Houze, 1993: Warm upper-level downdrafts associated with a squall line. *Mon. Wea. Rev.*, **121,** 2919-2927.

Trier, S.B., W.C. Skamarock, and M.A. LeMone, 1997: Structure and evolution of the 22 February 1993 TOGA COARE squall line: Organization mechanisms inferred from numerical simulations. *J. Atmos. Sci.*, **54,** 386-407.

Verlinde, J., and W.R. Cotton, 1990: A mesoscale vortex couplet observed in the trailing anvil of a multicellular convective complex. *Mon. Wea. Rev.*, **118,** 993-1010.

Weisman, M.L., 1992: The role of convectively generated rear-inflow jets in the evolution of long-lived mesoconvective systems. *J. Atmos. Sci.*, **49,** 1826-1847.

_____, 1993: The genesis of severe, long-lived bow echoes. *J. Atmos. Sci.*, **50,** 645-670.

_____, 2001: Bow echoes: A tribute to T.T. Fujita. *Bull. Amer. Meteor. Soc.*, **82,** 97-116.

_____, and C.A. Davis, 1998: Mechanisms for the generation of mesoscale vortices within quasi-linear convective systems. *J. Atmos. Sci.*, **55,** 2603-2622.

_____, J.B. Klemp, and R. Rotunno, 1988: Structure and evolution of numerically simulated squall lines. *J. Atmos. Sci.*, **45,** 1990-2013

Zhang, D.-L., K. Gao, and D.B. Parsons, 1989: Numerical simulation of an intense squall line during 10-11 June 1985 PRE-STORM. Part I: Model verification. *Mon. Wea. Rev.*, **117,** 960-994.